PCCP

RSC Publishing

PAPER

View Article Online
View Journal | View Issue

Cite this: *Phys. Chem. Chem. Phys.*, 2013, **15**, 5553

Analysis of sensitivity enhancement by dynamic nuclear polarization in solid-state NMR: a case study of functionalized mesoporous materials

Takeshi Kobayashi,[a] Olivier Lafon,[b] Aany S. Lilly Thankamony,[b] Igor I. Slowing,[a] Kapil Kandel,[af] Diego Carnevale,[c] Veronika Vitzthum,[c] Hervé Vezin,[d] Jean-Paul Amoureux,[b] Geoffrey Bodenhausen[ce] and Marek Pruski*[af]

Received 5th January 2013,
Accepted 29th January 2013

DOI: 10.1039/c3cp00039g

www.rsc.org/pccp

We systematically studied the enhancement factor (per scan) and the sensitivity enhancement (per unit time) in ^{13}C and ^{29}Si cross-polarization magic angle spinning (CP-MAS) NMR boosted by dynamic nuclear polarization (DNP) of functionalized mesoporous silica nanoparticles (MSNs). Specifically, we separated contributions due to: (i) microwave irradiation, (ii) quenching by paramagnetic effects, (iii) the presence of frozen solvent, (iv) the temperature, as well as changes in (v) relaxation and (vi) cross-polarization behaviour. No line-broadening effects were observed for MSNs when lowering the temperature from 300 to 100 K. Notwithstanding a significant signal reduction due to quenching by TOTAPOL radicals, DNP-CP-MAS at 100 K provided global sensitivity enhancements of 23 and 45 for ^{13}C and ^{29}Si, respectively, relative to standard CP-MAS measurements at room temperature. The effects of DNP were also ascertained by comparing with state-of-the-art two-dimensional heteronuclear $^{1}H\{^{13}C\}$ and $^{29}Si\{^{1}H\}$ correlation spectra, using, respectively, indirect detection or Carr–Purcell–Meiboom–Gill (CPMG) refocusing to boost signal acquisition. This study highlights opportunities for further improvements through the development of high-field DNP, better polarizing agents, and improved capabilities for low-temperature MAS.

1. Introduction

One of the most fundamental challenges in nuclear magnetic resonance (NMR) is its intrinsically low sensitivity. The signal-to-noise ratio (S/N) per scan in an NMR measurement depends upon, among other parameters, the gyromagnetic ratio of the observed nuclei γ_{obs}, the strength of the static magnetic field B_0, the temperature T and the apparent transverse relaxation time, T_2^*.[1] In solid-state NMR, the detection limits are further affected by inhomogeneous line broadening, which can reduce T_2^* by several orders of magnitude.

One of the main strategies for increasing the sensitivity is to begin by exciting high-γ spins and transferring their polarization to the observed low-γ nuclei. This approach is commonly used in $^{1}H \rightarrow X$ cross-polarization (CP), as a means of improving the sensitivity of hetero-nuclei (X = ^{13}C, ^{29}Si, ^{15}N, *etc.*) in solids. Correspondingly larger gains of up to two orders of magnitude can be achieved by polarizing the nuclei *via* unpaired electron spins, as proposed by Overhauser and demonstrated by Slichter in the 1950s.[2,3] This idea, referred to as dynamic nuclear polarization (DNP), relies on the transfer of polarization from unpaired electrons to nuclei, which is driven by microwave (μw) irradiation near the electron spin resonance (ESR) frequency. In the 1980s and 1990s DNP was combined with $^{1}H \rightarrow X$ CP under magic angle spinning (MAS), and applied successfully to a variety of solid materials containing unpaired electrons that occur naturally or are introduced by doping.[4,5] In the past decade, advances in gyrotron technology,[6,7] the development of cryogenic MAS probes for DNP,[8] and improved biradicals or other polarizing agents[9–11] enabled researchers to perform DNP

[a] *U.S. Department of Energy, Ames Laboratory, Ames, Iowa 50011, USA*
[b] *Université de Lille Nord de France, 59000 Lille, CNRS UMR 8181, Unité de Catalyse et de Chimie du Solide (UCCS), Ecole Nationale Supérieure de Chimie de Lille, Université de Lille 1, 59652 Villeneuve d'Ascq, France*
[c] *Institut des Sciences et Ingénierie Chimiques, Ecole Polytechnique Fédérale de Lausanne, EPFL, Batochime, 1015 Lausanne, Switzerland*
[d] *Université de Lille Nord de France, 59000 Lille, CNRS UMR 8516, Laboratoire de Spectrochimie Infrarouge et Raman (LASIR), Université de Lille 1, 59652 Villeneuve d'Ascq, France*
[e] *Département de Chimie, Ecole Normale Supérieure, Université Pierre et Marie Curie, CNRS UMR 7203, Paris, France*
[f] *Department of Chemistry, Iowa State University, Ames, Iowa 50011, USA. E-mail: mpruski@iastate.edu*

NMR experiments at higher magnetic fields. One of the most universal polarizing agents is the biradical 1-(TEMPO-4-oxy)-3-(TEMPO-4-amino)propan-2-ol (TOTAPOL).[10] For favourably oriented molecules in frozen glasses, the two unpaired electrons of TOTAPOL exhibit ESR frequencies that differ roughly by the nuclear Larmor frequency.[12] This facilitates an efficient three-spin "cross-effect" involving a flip-flop process of the two unpaired electrons and a flip of the nucleus.[12–14] Significant signal enhancements can be achieved, not only in biological systems[8,15–20] but also in microcrystalline organic solids[21,22] or on surfaces and subsurfaces of silicates, aluminates, nanomaterials, and metal–organic frameworks (MOFs).[23–26]

Several studies have addressed the quantification of the sensitivity enhancement in these experiments.[21,26–30] The DNP enhancement factor is typically determined by comparing the spectra measured with μw irradiation "on" and "off", under the same conditions of static field B_0 and sample temperature T, using sufficiently long recycle delays so that relaxation effects can be neglected. In a study of DNP-enhanced ^{13}C CP-MAS NMR of a solvent-free peptide with covalently attached TOTAPOL[28] a more general enhancement factor was described which also accounts for effects of the radicals on the spin-lattice relaxation times $T_1{}^{\mathrm{H}}$ of the protons and on paramagnetic broadening ('quenching') of the signals. The influence of TOTAPOL concentration (in water/glycerol) on $T_1{}^{\mathrm{H}}$ and $T_{1\rho}{}^{\mathrm{H}}$ relaxation of protons, and the performance of ^{13}C DNP-CP-MAS NMR in proline was studied by Lange *et al.*[30] Rossini *et al.*[29] quantified sensitivity enhancements of ^{29}Si DNP-CP-MAS NMR of passivated hybrid mesoporous silica. In addition to quenching and $T_1{}^{\mathrm{H}}$ relaxation, they studied the effect of TOTAPOL on T_2' dephasing times of the ^{29}Si nuclei in $^1\mathrm{H} \rightarrow {}^{29}\mathrm{Si}$ CP-MAS and demonstrated that further signal enhancement is possible in DNP-CP-MAS experiments by multiple refocusing using Carr–Purcell–Meiboom–Gill (CPMG) sequences. Very recently, Takahashi *et al.*[21] compared the sensitivity of ^{13}C DNP-CP-MAS and conventional CP-MAS for [2-^{13}C]glycine and microcrystalline cellulose. These recent studies have highlighted the importance of optimizing the sensitivity, $(\mathrm{S/N})^{\mathrm{time}}$, defined as S/N per square root of unit time, rather than the enhancement per scan. Paramagnetic doping can have positive or deleterious effects: increasing the signal per observed spin and allowing for shorter recycle delays on the one hand, and quenching and broadening the signals on the other. Thus, careful sample preparation and optimization of the experimental conditions are critical.

Here, we set out to systematically assess the contributions of various experimental factors to the global sensitivity enhancement in DNP-CP-MAS NMR of both ^{13}C and ^{29}Si nuclei. We focus on mesoporous silica nanoparticles (MSNs) functionalized with 3-(*N*-phenylureido)propyl (PUP) groups. In particular, we compare signals obtained under optimized DNP conditions and signals achievable at room temperature with non-impregnated samples exposed to ambient conditions in the laboratory (hereafter, "dry"). We take into account differences in relaxation, polarization transfer, and the chemical environment. Furthermore, we correlate these capabilities with state-of-the-art two-dimensional (2D) heteronuclear correlation (HETCOR) spectra utilizing either indirect detection of ^{13}C nuclei *via* protons,[31,32] or CPMG-enhanced ^{29}Si acquisition.[33,34] The discussion also incorporates contributions to the global sensitivity enhancement that were not addressed experimentally, stemming from potential changes in line widths, solvent effects, the Boltzmann factor, and probe characteristics. The results of this study offer additional insights into the potential of DNP for functionalized surfaces and highlight the need for further improvements.

2. Experimental

2.1. Materials

The PUP-functionalized MSNs (PUP-MSNs) were prepared using a previously reported co-condensation method.[35,36] Cetyltrimethylammonium bromide (CTAB), sodium hydroxide, aniline and mesitylene were purchased from Sigma-Aldrich. Tetraethoxysilane (TEOS) and 3-isocyanatopropyl-triethoxysilane were purchased from Gelest. All reagents were used as received. 3-Isocyanatopropyl triethoxysilane (0.50 mL) was mixed with aniline (0.25 mL) in a screw-cap vial and stirred at room temperature for 1 h to give crude 3-(*N*-phenylureido)propyl triethoxysilane. Simultaneously, CTAB (1.02 g), mesitylene (5.0 mL), NaOH (2 M, 3.5 mL), and H_2O (480 mL) were mixed in a round-bottom flask and heated at 80 °C for 1 h with vigorous stirring. To the resulting clear solution, TEOS (5.0 mL) was added drop-wise followed immediately by drop-wise addition of the crude 3-(*N*-phenylureido)propyl triethoxysilane, forming a cream-colored precipitate. The product was isolated by hot filtration, washed with copious amounts of water and methanol, and dried under vacuum at room temperature. The template was extracted by refluxing methanol in a Soxhlet extractor. The resulting surfactant-free solid product was dried under vacuum at room temperature. The concentration of PUP groups was estimated at 1.3 (±0.1) mmol/g, based on quantitative ^{29}Si NMR spectrum taken using direct polarization.

2.2. Solid-state NMR

2.2.1. Sample preparation. Dry PUP-MSN powder was mixed with 12.5 mM TOTAPOL dissolved in water with natural isotopic abundance and stirred using a glass rod. This concentration is known to result in optimal sensitivity enhancements for mesoporous silica materials.[29] After one day of impregnation at room temperature, excess TOTAPOL solution was removed by centrifugation at 12110 × *g* for 5 min. The concentration of TOTAPOL in the samples was measured on a Bruker Biospin ELEXYS E580E X-band ESR spectrometer, using 2 mW of μw power, 0.5 G amplitude modulation, and 4-amino-TEMPO as reference. The ESR spectrum was simulated with the EasySpin program[37] knowing the *g*-tensor, the hyperfine couplings with the ^{14}N nucleus, the dipolar interaction between the two electrons of TOTAPOL and the rotational correlation time, τ_c. To assess the extent of paramagnetic quenching, the PUP-MSN powder was also impregnated with pure water in natural isotopic abundance, following the same procedures. The impregnated

samples were transferred to 3.2-mm sapphire rotors and weighed. Sapphire is nearly transparent to frequencies higher than 140 GHz and its excellent thermal conductivity reduces the sample heating due to μw irradiation and MAS.[38,39]

2.2.2. DNP NMR measurements. One-dimensional (1D) $^{1}H \rightarrow {}^{13}C$ and $^{1}H \rightarrow {}^{29}Si$ solid-state NMR CP-MAS spectra were obtained at B_0 = 9.4 T (400 MHz for protons) using a Bruker BioSpin DNP NMR spectrometer, equipped with a gyrotron generating a continuous-wave power of 5 W at 263 GHz. The μw irradiation was transmitted through a corrugated waveguide to a triple resonance $^{1}H/X/Y$ MAS probe for 3.2 mm rotors spinning at a MAS frequency ν_R = 10 kHz.[10,40] NMR spectra with μw irradiation ''on'' or ''off'' were acquired at a temperature T = 98 K, which was stabilized using a Bruker BioSpin MAS cooling system.

2.2.3. Other solid-state NMR measurements. Additional 1D $^{1}H \rightarrow {}^{13}C$ and $^{1}H \rightarrow {}^{29}Si$ CP-MAS experiments were performed at 9.4 T on a Chemagnetics Infinity spectrometer with samples in 5 mm zirconia rotors spinning at 10 kHz. Their temperature was adjusted to T = 120 or 310 K by employing the Chemagnetics variable temperature system and calibrated with ±5 K accuracy using KBr as external reference.[41] The CP transfers were optimized separately in all experiments.

All $^{1}H \rightarrow {}^{13}C \rightarrow {}^{1}H$ and $^{1}H \rightarrow {}^{29}Si$ 2D HETCOR spectra were recorded at room temperature on a Varian NMR spectrometer at 14.1 T (600 MHz for protons) equipped with a MAS probe with 1.6 mm rotors spinning at ν_R = 40 kHz. The sensitivity of these experiments was improved by indirect detection *via* protons for heteronuclear $^{1}H-{}^{13}C$ correlation and multiple CPMG refocusing for $^{1}H-{}^{29}Si$ correlation.[31–34]

The experimental parameters are given in the captions, using the following symbols: ν_{RF}^{X} is the magnitude of the radiofrequency (RF) magnetic field applied to X spins, τ_{CP} is the cross-polarization time, τ_{CPMG} is the delay between the rotor-synchronized π pulses in the CPMG sequence, N_{CPMG} is the number of echoes, Δt_1 is the increment of t_1 during 2D acquisition, and τ_{RD} is the recycle delay (we assume that the acquisition time of free induction decay is negligibly small compared to the recovery delay). The ^{1}H, ^{13}C and ^{29}Si chemical shifts were referenced with respect to tetramethylsilane (TMS) at 0 ppm.

3. Results

The overall concentration of TOTAPOL, c_m, in the impregnated PUP-MSNs was determined by ESR spectroscopy and is about 9.5 mM. The simulation of the X-band ESR spectrum (not shown) yields a correlation time τ_c = 410 ns,[42] which indicates that the motions of the TOTAPOL molecules are strongly restricted in the mesopores of MSNs. This observation suggests some adsorption of TOTAPOL onto the silica surface.[25] The parameters extracted from the fit of the X-band ESR spectrum were used to simulate the ESR spectrum at 263 GHz which exhibits a 1.1 GHz inhomogeneous broadening due to *g*-anisotropy. This greatly exceeds the ^{1}H Larmor frequency at 9.4 T and favours the cross-effect DNP mechanism involving two unpaired electrons in TOTAPOL.[12–14,39,43] The amplitude of the microwave field in the sample does not exceed a few MHz,[44] thus only a small fraction of the unpaired electrons can be saturated by the microwave irradiation in a static sample. However, in a spinning sample the ESR resonance frequencies are modulated by the sample rotation, so that a larger fraction of unpaired electrons can be affected by the microwave field, thereby contributing to the DNP enhancement.[45,46]

Table 1 Summary of samples and experimental conditions used in $^{1}H \rightarrow {}^{13}C$ and $^{1}H \rightarrow {}^{29}Si$ CP-MAS experiments at 9.4 T

Experiment[a]	Solvent	T [K]	TOTAPOL	μw
H_2O*-LT-on	H_2O	98	Yes	On
H_2O*-LT-off	H_2O	98	Yes	Off
H_2O-LT-off	H_2O	120	No	Off
Dry-LT-off	None	120	No	Off
Dry-RT-off	None	310	No	Off

[a] H_2O: samples with H_2O, dry: samples without solvent exposed to ambient conditions in the laboratory, '*': samples with TOTAPOL, LT: low temperature, RT: room temperature, 'on': with μw irradiation, 'off': without μw irradiation.

To separate various contributions to the global DNP enhancement, we carried out a series of $^{1}H \rightarrow {}^{13}C$ and $^{1}H \rightarrow {}^{29}Si$ CP-MAS experiments using the samples and experimental conditions summarized in Table 1.

Fig. 1 shows $^{1}H \rightarrow {}^{13}C$ and $^{1}H \rightarrow {}^{29}Si$ CP-MAS spectra of H_2O*-LT-on and H_2O*-LT-off. The first spinning sideband (SSB) of the aromatic carbons overlaps with aliphatic signals. Fig. 1 clearly demonstrates the DNP enhancement per scan (see eqn (1)) in both ^{13}C and ^{29}Si spectra ($\varepsilon_{on/off}^{scan} \approx 23$ for both nuclei).

As expected, the longitudinal relaxation times $T_1{}^{H}$ of the proton bath, summarized in Table 2, are strongly influenced by

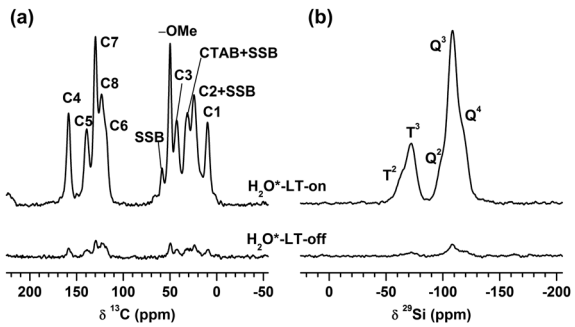

Fig. 1 (a) $^{1}H \rightarrow {}^{13}C$ and (b) $^{1}H \rightarrow {}^{29}Si$ CP-MAS spectra of PUP-MSNs impregnated with aqueous TOTAPOL solution, recorded with and without μw irradiation at $T \approx 98$ K (H_2O*-LT-on and H_2O*-LT-off, respectively). The spectra were measured using ν_R = 10 kHz, τ_{CP} = 2 ms, $\nu_{RF}^{C} = \nu_{RF}^{Si}$ = 46 kHz during CP, ν_{RF}^{H} ramped from 53 to 59 kHz during CP and ν_{RF}^{H} = 95 kHz during the π/2 pulses and SPINAL-64 ^{1}H decoupling.[47] The recycle delay was τ_{RD} = 1.3 s, 512 scans were accumulated for ^{13}C (total time = 11 min) and 1024 scans for ^{29}Si (total time = 22 min). The ^{13}C signal assignments in PUP refer to Scheme 1. ''CTAB'' denotes the CH_2 resonances of the residual cetyltrimethylammonium bromide surfactant that was not extracted from the pores, whereas ''-OMe'' represents methoxy groups due to washing with methanol. In (b), the T^n silicon signals with n = 2 or 3 represent $(SiO)_n$**Si**R$(OX)_{3-n}$ grafting sites with R = PUP, X = H or Me, whereas Q^n (n = 2, 3 and 4) corresponds to $(SiO)_n$**Si**$(OX)_{4-n}$ sites.

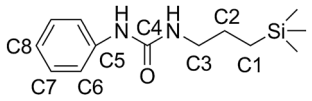

Scheme 1 The PUP functional group.

Table 2 Proton longitudinal relaxation times T_1^H at around 100 K and 9.4 T

Experiment	T_1^H (s)
H_2O*-LT-off	1.1
H_2O-LT-off	4.0
Dry-LT-off[a]	0.17
Dry-RT-off[a]	1.2

[a] Samples were handled in an ambient atmosphere.

the radicals, solvent, and temperature.[28,29] The relaxation was mono-exponential in all samples. The difference in relaxation times between dry-LT-off and dry-RT-off is attributed to the reduction of the mobility of the PUP and silanol groups at 120 K compared to 310 K.

No difference in line broadening was observed in $^1H \rightarrow {}^{13}C$ and $^1H \rightarrow {}^{29}Si$ CP-MAS spectra with and without μw irradiation (see Fig. 1). This can be ascribed to (i) the propagation of DNP-enhanced ^1H polarization *via* ^1H spin diffusion, as previously observed in organic and hybrid nano- and micro-particles,[15,22,42] and (ii) the low efficiency of CP in the vicinity of TOTAPOL, owing to short longitudinal and $T_{1\rho}{}^H$ relaxation times in the rotating frame.[30] Nuclei in the immediate proximity of TOTAPOL radicals (on the order of ~1 nm or less)[30,48] are not observable ('quenched') because of paramagnetic broadening. Furthermore, Fig. 2 shows that TOTAPOL did not broaden the visible linewidths at the concentrations used in this study. This is due both to the low CP efficiency near TOTAPOL and to the atomic-scale disorder in PUP-MSNs, producing a distribution in ^{13}C and ^{29}Si isotropic chemical shifts, which masks paramagnetic broadening.

Fig. 3 compares the intensities of $^1H \rightarrow {}^{13}C$ and $^1H \rightarrow {}^{29}Si$ CP-MAS spectra of the samples dry-RT-off, dry-LT-off and H_2O-LT-off, collected using $\tau_{RD} > 3T_1{}^H$. The measurements were performed at 9.4 T on a Chemagnetics spectrometer. For comparison between the two 9.4 T spectrometers, the $^1H \rightarrow {}^{13}C$ and $^1H \rightarrow {}^{29}Si$ CP-MAS spectra of the H_2O-LT-off sample were recorded on both instruments (see Fig. 2 and top spectra of Fig. 3). The RF amplitudes of the ^1H decoupling fields were 95 and ~40 kHz, respectively, on the spectrometers with and without gyrotron, hence the broadening of the aliphatic carbon signals observed without gyrotron. Fig. 3 shows that the presence of frozen water does not increase the linewidth in PUP-MSN, since the dry PUP-MSNs already exhibit atomic-scale disorder. This observation stands in contrast with organic or biological molecules in frozen solutions, where significant line broadening due to static disorder in frozen samples has been reported.[49]

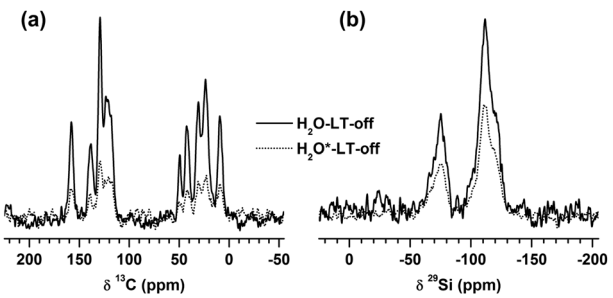

Fig. 2 (a) $^1H \rightarrow {}^{13}C$ and (b) $^1H \rightarrow {}^{29}Si$ CP-MAS spectra of PUP-MSNs without TOTAPOL (H_2O-LT-off, solid) and with TOTAPOL (H_2O*-LT-off, dotted). The recycle delays were τ_{RD} = 5 s for H_2O*-LT-off and τ_{RD}=15 s for H_2O-LT-off, with 512 scans acquired for both ^{13}C spectra and the ^{29}Si spectrum H_2O-LT-off, and 3072 scans for the ^{29}Si spectrum H_2O*-LT-off. The other experimental conditions were the same as in Fig. 1. The spectra were normalized by dividing the intensities by the number of scans to compare intensities per scan.

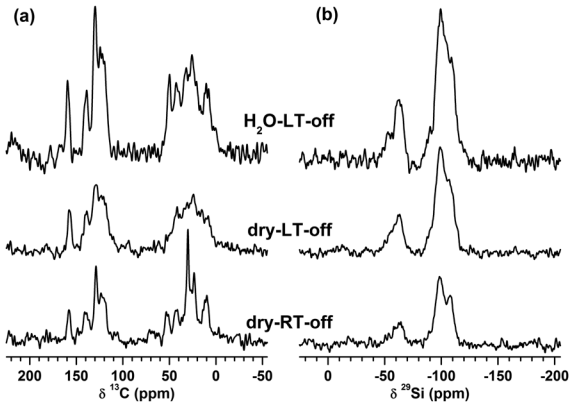

Fig. 3 (a) $^1H \rightarrow {}^{13}C$ and (b) $^1H \rightarrow {}^{29}Si$ CP-MAS spectra of H_2O-LT-off (top), dry-LT-off (middle), and dry-RT-off (bottom), acquired on a 9.4 T spectrometer without gyrotron using ν_R = 10 kHz, ν_{RF}^H = 40 kHz during CP and TPPM decoupling, and $\nu_{RF}^C = \nu_{RF}^{Si}$ = 50 kHz during CP. Other experimental conditions were: τ_{RD} = 30 s, τ_{CP} = 0.5 ms for ^{13}C and 5 ms for ^{29}Si (H_2O-LT-off); τ_{RD} = 1 s, τ_{CP} = 1 ms for ^{13}C and 5 ms for ^{29}Si (dry-LT-off); τ_{RD} = 3.5 s, τ_{CP} = 1 ms for ^{13}C and 7 ms for ^{29}Si (dry-RT-off). The spectra were normalized to compare intensities per scan.

4. Discussion

4.1. Contributions to the global DNP enhancement

When comparing DNP-CP-MAS with traditional CP-MAS measurements, one must consider not only the effect of μw irradiation on the nuclear polarization, but also the consequences of introducing the TOTAPOL solution into the pores. As noted above, TOTAPOL enhances nuclear T_1 relaxation, thereby allowing for shorter recycle delays, so that more scans can be recorded per unit time. On the other hand, the unpaired electrons can render a fraction of the nuclei unobservable due to paramagnetic broadening. The frozen solvent (water in our case) modifies the environment of the nuclei and provides an abundant pool of ^1H nuclei in the pores. This affects the longitudinal relaxation times $T_1{}^H$, as well as the efficiency of the CP process.[30] The discussion below includes several additional factors that were not confronted experimentally.

4.1.1. Enhancement per scan and per unit of time. When comparing two experiments A and B, the improvement in S/N can be characterized in terms of an enhancement factor either

per scan (ε^{scan}) or *per unit of experimental time* (ε^{time}). The former is defined as the ratio of S/N for long recovery delays

$$\varepsilon^{scan}(A;B) = \frac{S_A(\infty)}{S_B(\infty)}\frac{N_B}{N_A}, \quad (1)$$

where, N_A and N_B are the root-mean-square (rms) amplitudes of the noise in experiments A and B, $S_A(\infty)$ and $S_B(\infty)$ are the signal intensities per scan of experiments A and B measured with recycle delays $\tau_{RD}(A) > 5T_1(A)$ and $\tau_{RD}(B) > 5T_1(B)$, with $T_1(A)$ and $T_1(B)$ being the relevant time constants of the build-up of the nuclear polarization, either towards Boltzmann equilibrium, or towards the DNP-enhanced polarization. The expression of ε^{scan} in the case of partial saturation ($\tau_{RD}(A) < 5T_1(A)$ and $\tau_{RD}(B) < 5T_1(B)$) is derived in Appendix A.1. If the rms amplitudes of the noise are identical in experiments A and B ($N_A = N_B$), $\varepsilon^{scan}(A; B)$ is equal to the ratio of signal intensities, $S_A(\infty)$ and $S_B(\infty)$.

In the presence of line broadening, one should separate the contributions to the enhancement factor, ε^{scan}, due to the integrated intensities, $\varepsilon^{integral}$, the line widths, ε^{LW}, and the noise, ε^{noise}. In the Appendix A.2, we show that

$$\varepsilon^{scan}(A; B) = \varepsilon^{integral}(A; B)\, \varepsilon^{LW}(A; B)\, \varepsilon^{noise}(A; B). \quad (2)$$

However, $\varepsilon^{scan}(A; B)$ does not take into account the changes in T_1 relaxation between experiments A and B. To quantify this contribution, we must consider the *sensitivity enhancement per unit time*:

$$\varepsilon^{time}(A;B) = \frac{S_A(\infty)}{S_B(\infty)}\frac{N_B}{N_A}\sqrt{\frac{T_1(B)}{T_1(A)}} = \varepsilon^{scan}(A;B)\sqrt{\kappa(A;B)} \quad (3)$$

as shown in Appendix A.3. In eqn (3), the factor $\kappa(A; B) = T_1(B)/T_1(A)$ is the ratio of longitudinal relaxation times in experiments B and A. For example, in $^1H \rightarrow X$ CP-MAS experiments, $\kappa = T_1^H(B)/T_1^H(A)$.

In the next paragraphs we discuss various contributions to the global sensitivity enhancement offered by DNP-CP-MAS experiments.

4.1.2. Microwave effect. The effect of μw irradiation is given by

$$\varepsilon_{on/off} = \varepsilon(H_2O^*\text{-LT-on}; H_2O^*\text{-LT-off}). \quad (4)$$

In $^1H \rightarrow {}^{13}C$ and $^1H \rightarrow {}^{29}Si$ DNP-CP-MAS experiments, the factor $\varepsilon^{scan}_{on/off}$ depends on the efficiency of (i) the polarization transfer between unpaired electrons and protons located near the spin diffusion barrier,[43,50,51] and of (ii) the propagation of DNP-enhanced ^1H polarization *via* ^1H–^1H spin diffusion.[15,22,42] Furthermore, in our PUP-MSN samples, as can be seen in Fig. 1, the μw irradiation affects neither the full width at half maximum (FWHM) nor the noise amplitude. The enhancement per scan, $\varepsilon^{scan}_{on/off} = 23$, which is identical for both $^1H \rightarrow {}^{13}C$ and $^1H \rightarrow {}^{29}Si$ CP-MAS spectra, indicates that the ^1H polarization is identical near various ^{13}C and ^{29}Si nuclei.[42] We have also verified that at 98 K the time constant of the polarization build-up, τ_{DNP}, is equal to the longitudinal proton relaxation time $T_1^H(H_2O^*\text{-LT-off})$, which is consistent with the assumption that the cross-effect is dominant in our samples (hence $\kappa_{on/off} = T_1^H(H_2O^*\text{-LT-off})/\tau_{DNP} = 1$).[27,29,49,52] (We note that diverging values of τ_{DNP} and T_1^H have been observed at temperatures below 30 K in samples containing frozen glassy solutions of TEMPO radicals.[53,54]) Thus, the effect of the recycle delay τ_{RD} does not depend on μw irradiation, and the sensitivity enhancement can be obtained by direct comparison of signal intensities observed in experiments H_2O^*-LT-on and H_2O^*-LT-off, hence $\varepsilon^{time}_{on/off} = \varepsilon^{scan}_{on/off} = 23$ for both ^{13}C and ^{29}Si.

4.1.3. Effect of radical concentration. The incorporation of TOTAPOL reduces the longitudinal proton relaxation time T_1^H, but also the apparent transverse relaxation time T_2^* of nearby nuclei, leading to line-broadening known as 'quenching' since it usually prevents the observation of nuclei distant by less than a few Angstroms from unpaired electrons. Furthermore, the introduction of exogenous radicals also shortens the longitudinal relaxation times in the rotating frame, $T_{1\rho}$, of both ^1H and X nuclei, which affects the CP efficiency. These paramagnetic effects can be assessed globally by comparing experiments with and without radicals,

$$\varepsilon_{para} = \varepsilon(H_2O^*\text{-LT-off}; H_2O\text{-LT-off}). \quad (5)$$

As stated in the previous section (see Fig. 2), the introduction of TOTAPOL into our PUP-MSN samples affects neither the linewidths of ^{13}C and ^{29}Si signals nor the noise. However, the quenching and magnetization losses during CP due to radicals[30] are severe, resulting in $\varepsilon^{scan}_{para}(^{13}C) = 0.25$. For ^{29}Si nuclei, three independent measurements at 9.4 T yielded $\varepsilon^{scan}_{para}(^{29}Si) = 0.59$, 0.58 and 0.51. Therefore, we use the value of 0.58 here. However, the effect of quenching is partly compensated by the acceleration of the T_1^H relaxation, since $\kappa_{para} = T_1^H(H_2O\text{-LT-off})/T_1^H(H_2O^*\text{-LT-off}) = 3.6$, so that $\sqrt{\kappa_{para}} = 1.9$. The factor $\varepsilon^{time}_{para}$ can be estimated using the measured S/N ratios and eqn (3) to be $\varepsilon^{time}_{para} = 0.25\sqrt{3.6} = 0.48$ and $0.58\sqrt{3.6} = 1.1$ for ^{13}C and ^{29}Si, respectively. Assuming that (i) the TOTAPOL molecules are homogeneously distributed in frozen water (which at the concentration of 9.5 mM corresponds to one biradical molecule per ~175 nm^3), (ii) the unpaired electrons in TOTAPOL are roughly 1 nm apart, and (iii) the quenching affects all nuclei closer than 1 nm from the unpaired electrons,[30] the expected values of $\varepsilon^{scan}_{para}$ should exceed 0.9. The fact that more significant fractions of both nuclei became ''invisible'' in our experiments can be attributed to the large pore diameter (~5 nm) of the MSNs used in this study, which enabled the penetration of TOTAPOL biradicals into the pores. Furthermore, it has been suggested that TOTAPOL radicals may be adsorbed on the surface *via* hydrogen bonds with silanol and siloxane groups.[25] Such an adsorption can amplify the quenching effect. We also note that the values of $\varepsilon^{scan}_{on/off}(^{29}Si)$ and $\varepsilon^{scan}_{para}(^{29}Si)$ observed for ^{29}Si nuclei in our PUP-MSN samples are in good agreement with those reported by Emsley and co-workers for a TOTAPOL concentration of ~8 mM in methyl passivated SBA-15 silica.[29] For a concentration that matches ours (~9.5 mM), they reported a higher enhancement factor $\varepsilon^{scan}_{on/off}(^{29}Si) = 33$ but a more pronounced signal loss $\varepsilon^{scan}_{para}(^{29}Si) = 0.39$ due to the radicals. The significant decrease in NMR signals owing to the

presence of TOTAPOL in our samples highlights the need to avoid close contacts of TOTAPOL with the target spins.[42]

4.1.4. Effect of solvents. The presence of frozen solvent (here water) affects both the signal intensity and the $T_1{}^H$ relaxation. These effects are quantified by the factor

$$\varepsilon_{solvent} = \varepsilon(H_2O\text{-LT-off; dry-LT-off}) \quad (6)$$

based on spectra such as shown in Fig. 3. In Fig. 3, the ^{13}C signals from aliphatic carbons in both H_2O-LT-off and dry-LT-off show increased line widths with respect to H_2O-LT-off spectra in Fig. 2, owing to insufficient amplitude of the ^1H decoupling field. To avoid errors due to insufficient decoupling, the enhancements per scan were evaluated using the integrated intensities of signals of aromatic carbons, which can be decoupled with weaker RF fields. In principle, the factor $\varepsilon_{solvent}^{scan}$ incorporates effects of sample dilution and modifications in CP efficiency due to the change in ^1H density around the detected nuclei. For porous solids such as PUP-MSNs, the impregnation with solvent sets a limit to the dilution and the presence of a larger ^1H bath of frozen water improves the CP efficiency per scan,[39] resulting in enhancement factors $\varepsilon_{solvent}^{scan}(^{13}C) = 2.4$ and $\varepsilon_{solvent}^{scan}(^{29}Si) = 1.6$. However, the $T_1{}^H$ relaxation was slowed down by the presence of frozen water ($\kappa_{solvent} = T_1{}^H$(dry-LT-off)/$T_1{}^H$($H_2O$-LT-off) = 0.04 according to Table 2). Thus the sensitivity per unit time is *decreased* for both nuclei (eqn (3) yields $\varepsilon_{solvent}^{time}(^{13}C) = 0.49$ and $\varepsilon_{solvent}^{time}(^{29}Si) = 0.33$).

4.1.5. Enhancement with respect to low temperature CP-MAS. Since the three contributions described by eqn (4) to (6) act in concert during the DNP experiment, the enhancement per scan between H_2O*-LT-on and dry-LT-off experiments is given by

$$\varepsilon_{DNP}^{scan} = \varepsilon_{on/off}^{scan}\, \varepsilon_{para}^{scan}\, \varepsilon_{solvent}^{scan}. \quad (7)$$

The corresponding sensitivity enhancement is

$$\varepsilon_{DNP}^{time} = \varepsilon_{DNP}^{scan}\sqrt{\kappa_{DNP}} \quad (8)$$

with

$$\kappa_{DNP} = \kappa_{on/off}\kappa_{para}\kappa_{solvent}, \quad (9)$$

where $\kappa_{DNP} = T_1{}^H$(dry-LT-off)/τ_{DNP}. Eqn (7) yields $\varepsilon_{DNP}^{scan}(^{13}C) = 14$ and $\varepsilon_{DNP}^{scan}(^{29}Si) = 21$ for PUP-MSNs. Due to the short $T_1{}^H$ in the dry-LT-off experiment, the sensitivity enhancement was reduced with respect to that per scan to $\varepsilon_{DNP}^{time}(^{13}C) = 5.5$ and $\varepsilon_{DNP}^{time}(^{29}Si) = 8.3$.

4.1.6. Global enhancement. Finally, the sensitivity of DNP experiments has to be compared with conventional NMR methods at room temperature, with state-of-the-art probes, fast spinning, optimal pulse sequences, and the highest available magnetic fields. The global S/N enhancement with respect to conventional NMR experiment can be evaluated as,

$$\varepsilon_{global}^{scan} = \varepsilon_{DNP}^{scan}\, \varepsilon_{probe}^{scan}\, \varepsilon_{seq}^{scan}\, \varepsilon_{B}^{scan}\, \varepsilon_{T}^{scan} \quad (10)$$

where ε_{DNP}^{scan} is given by eqn (7) and the factors $\varepsilon_{probe}^{scan}$, ε_{seq}^{scan}, ε_{B}^{scan} and ε_{T}^{scan} account for the changes in S/N produced by differences in instrumentation, pulse sequences, static magnetic field and sample temperature when comparing DNP and conventional NMR experiments. The resulting global sensitivity enhancement per unit time is

$$\varepsilon_{global}^{time} = \varepsilon_{global}^{scan}\sqrt{\kappa_{global}} \quad (11)$$

with

$$\kappa_{global} = \kappa_{DNP}\kappa_B\kappa_T, \quad (12)$$

where κ_B and κ_T account for the effects of the static magnetic field and temperature on $T_1{}^H$ relaxation. The factor $\varepsilon_{probe}^{scan}$ is determined by characteristics of the coil (geometry, filling factor, quality factor Q, and temperature) and the temperature and performance of the preamplifier. The factor ε_{seq}^{scan} is essential when comparing experiments acquired with different pulse sequences, for example with or without recording multiple echoes using the CPMG sequence. The magnetic field and the sample temperature can affect both the signal integral (*via* the Boltzmann factor) as well as the linewidth.

As an example, for PUP-MSN samples, we compared at the same static field the sensitivity of DNP-CP-MAS at low temperature and conventional CP-MAS at room temperature

$$\varepsilon_{global} = \varepsilon(H_2O^*\text{-LT-on; dry-RT-off}) \quad (13)$$

and

$$\kappa_{global} = T_1{}^H(\text{dry-RT-off})/\tau_{DNP}. \quad (14)$$

In this case, $\varepsilon_{seq}^{scan} = 1$ while the Boltzmann factor and the $T_1{}^H$ times are only influenced by the temperature, $\varepsilon_B^{scan} = 1$, $\varepsilon_T^{scan} = 3$, $\kappa_B = 1$ and $\kappa_T = T_1{}^H$(dry-LT-off)/$T_1{}^H$(dry-RT-off) = 7 (using the values of Table 2). We further assumed that $\varepsilon_{probe}^{scan} = 1$. By inserting the appropriate relaxation times, eqn (11) yields the global enhancement factors $\varepsilon_{global}^{time}(^{13}C) = 23$ and $\varepsilon_{global}^{time}(^{29}Si) = 45$, respectively. The time savings in PUP-MSNs are thus given by factors $(\varepsilon_{global}^{time})^2 = 529$ and 2015 for ^{13}C and ^{29}Si, respectively.

In our samples, no significant changes in line widths were observed between the different experiments (under proper decoupling) since the dry-PUP-MSN samples already exhibit significant atomic-scale disorder. In general, the line widths can be affected by different factors, including paramagnetic effects, static disorder of the solvent or slower molecular motions at low temperature, as indeed observed in biological or organic molecules dispersed in glass-forming solvents or in metal-oxide frameworks.[21,26,49,55] These modifications of the line widths can lead to ε_{para}^{LW}, $\varepsilon_{solvent}^{LW}$, or $\varepsilon_T^{LW} < 1$. For instance, for glycine in a glass-forming solvent, $\varepsilon_{para}^{LW}\, \varepsilon_{sovent}^{LW}\, \varepsilon_T^{LW} = 0.2$ has been reported.[21] The static magnetic field often affects the line widths in solids, especially for NMR spectra of quadrupolar nuclei and protons, as well as NMR signals dominated by a distribution of isotropic chemical shifts.

The individual contributions and their origins are summarized in Tables 3 and 4. Clearly, the sensitivity enhancements will vary depending on the chemical structure and morphology of the samples, *e.g.*, pore diameter, surface passivation with nonpolar groups, concentration and accessibility of TOTAPOL, and sample treatment, *e.g.*, removal of paramagnetic oxygen that

Table 3 Quantification of the individual contributions to S/N and sensitivity enhancement when comparing experiments A and B for PUP-MSN

			ε^{scan}		ε^{time}	
	Experiment A	Experiment B	^{13}C	^{29}Si	^{13}C	^{29}Si
On/Off	H_2O^*-LT-on	H_2O^*-LT-off	23	23	23	23
Para	H_2O^*-LT-off	H_2O-LT-off	0.25	0.58	0.48	1.1
Solvent	H_2O-LT-off	dry-LT-off	2.4	1.6	0.49	0.33
DNP	H_2O^*-LT-on	dry-LT-off	14	21	5.5	8.3
T	dry-LT-off	dry-RT-off	1.6	2.0	4.3	5.3
Global	H_2O^*-LT-on	dry-RT-off	22	43	23	45

may have a significant effect on $T_1{}^H$ relaxation.[29,56] Whatever the details may be, the time-savings offered by DNP for $^1H \rightarrow {}^{13}C$ and $^1H \rightarrow {}^{29}Si$ CP-MAS spectra of such materials are remarkable.

4.2. Sensitivity enhancement by other techniques

The DNP enhancements have so far been compared with conventional $^1H \rightarrow X$ CP-MAS experiments at around 100 and 300 K. However, several other approaches can be used to boost the sensitivity of standard NMR. In our earlier studies of organic–inorganic hybrid materials, we took advantage of $^1H \rightarrow {}^{13}C \rightarrow {}^1H$ indirectly detected heteronuclear correlation as well as CPMG-based detection of ^{29}Si nuclei.[33,34] Both of these approaches can be combined with DNP. Indeed, Emsley and coworkers have recently used CPMG sequences in 1D DNP-CP-MAS studies of functionalized silica, which yielded appreciable enhancements ε_{seq}^{scan} on the order of 2 to 5.[29] The use of indirect detection would benefit from further improvements of fast spinning at low temperatures. Here, we report 2D ^1H–^{13}C and ^1H–^{29}Si heteronuclear correlation spectra of the same PUP-MSN sample taken without the assistance of DNP under the best possible conditions currently available in our laboratories.

Fig. 4 shows 1D $^1H \rightarrow {}^{13}C$ CP-MAS spectra and 2D $^1H \rightarrow {}^{13}C \rightarrow {}^1H$ spectra of the dry-RT-off sample obtained at 14.1 T. Both data sets were acquired in *the same experimental time*. As expected, the 2D experiment provides useful ^1H–^{13}C correlations. More surprisingly, it also yields better S/N ratios for all carbons than the corresponding 1D CP-MAS spectrum (by a factor of $\sim$2 in the case of C7), thus clearly demonstrating the sensitivity advantage of indirect detection. The comparison with the 1D $^1H \rightarrow {}^{13}C$ DNP-CP-MAS spectrum (H_2O^*-LT-on, Fig. 1a) is not straightforward, due to different magnetic fields, different spinning frequencies, the presence of spinning sidebands in the DNP-enhanced spectrum, the use of two consecutive CP steps for indirect detection at room temperature,

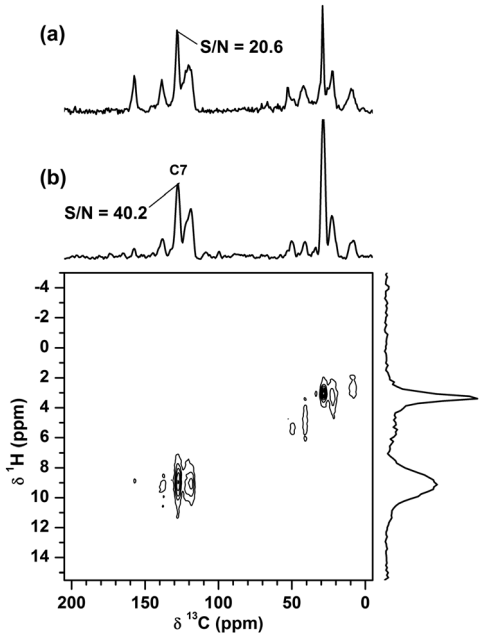

Fig. 4 (a) 1D $^1H \rightarrow {}^{13}C$ conventional CP-MAS spectrum and (b) indirectly detected 2D $^1H \rightarrow {}^{13}C \rightarrow {}^1H$ spectrum of PUP-MSNs measured at room temperature (dry-RT-off) at 14.1 T. The spectra were obtained with ν_R = 40 kHz, τ_{CP} = 1 ms, ν_{RF}^C = 100 kHz during short pulses and CP, ν_{RF}^H = 125 kHz during short pulses and 60 kHz during CP, recycle delay τ_{RD} = 1.5 s, $\nu_{RF}^H = \nu_{RF}^C$ = 10 kHz during SPINAL64 heteronuclear decoupling,[47] and acquisition time = 3 h 40 min in both experiments: 8600 scans in (a), and 128 increments with Δt_1 = 12.5 μs and 32 scans each in (b). The ^1H and ^{13}C projections in (b) are shown in 'skyline' mode, *i.e.* only the positive or negative intensities corresponding to the maximum absolute values are retained.

Table 4 Origin of the different contributions to sensitivity enhancement

	$\varepsilon^{integral}$	ε^{LW}	ε^{noise}	κ
On/Off	(i) e^-–^1H transfer (ii) ^1H–^1H spin diffusion	1[a]	1	1[b]
Para	(i) CP transfer (ii) Quenching	Paramagnetic broadening	1	Paramagnetic relaxation
Solvent	CP transfer	Static disorder	1	Reduced mobility
Probe	(i) Filling factor (ii) Q factor	Field homogeneity	Thermal noise	1
Seq.	Pulse sequence efficiency	1[c]	1[c]	1
B	Boltzmann	(i) $H_Q^{(2)}$[d] (ii) Distribution of δ_{iso} (iii) ^1H, ^{19}F spectra[e]	$\sqrt{B_0}$	Larmor frequency
T	(i) Boltzmann (ii) CP transfer	(i) Mobility (ii) Decoupling	1	Mobility

[a] Not necessarily when only a fraction of the sample is enhanced by DNP. [b] Valid for DNP by the 'cross-effect' and fast ^1H–^1H spin diffusion but not in all other cases.[22,52] [c] Not when the sequences differ by the RF irradiation during signal acquisition (use of hetero- or homo-nuclear decoupling, CPMG). [d] Second-order quadrupolar broadening. [e] Reduction of the line broadening due to homonuclear dipolar interactions for a larger difference in resonance frequencies.

the presence of frozen water and its rigidity at low temperatures, and different rotors with capacities of 160 and 8 μL at 9.4 and 14.1 T, respectively. Noting that the ^{13}C spectrum in Fig. 1a was acquired in just 11 min, while the spectra in Fig. 4 required 3 h and 40 min, it is clear that for 1D spectra, DNP-CP-MAS offers a sensitivity advantage over other approaches. However, the measurements of meaningful 2D correlations can be problematic under current DNP conditions because the frozen solvent affects the intermolecular interactions on the surface and, most importantly, participates in the cross-polarization process. In the best of possible worlds, one could envision a combination of indirect detection and solvent-free DNP.[57] This is worthy of pursuit and could greatly expand the limits of modern solid-state NMR.

For heteronuclear correlations of ^{1}H and ^{29}Si, it has been our experience that the sensitivity of indirect detection can be surpassed by direct CPMG-enhanced detection of ^{29}Si signals, which requires only a single CP step and takes advantage of the slow T_2' relaxation of ^{29}Si nuclei.[33,34,58,59] The 2D ^{1}H–^{29}Si CPMG-enhanced spectrum for dry-RT-off sample, processed as described earlier,[25] is shown in Fig. 5, along with 1D $^{1}H \rightarrow {}^{29}Si$ CP-MAS spectra acquired with and without CPMG under the same conditions at 300 K and 14.1 T. To avoid spectral distortions due to differences in T_2' of ^{29}Si nuclei,[34] only N_{CPMG} = 5 echoes were used, which was sufficient to give an enhancement ε_{seq}^{time}(dry-RT-off-CPMG; dry-RT-off) = 2.3 and a good 2D spectrum within a reasonable experimental time (~18 h). Such ^{1}H–^{29}Si HETCOR spectra are useful to characterize the conformations of functional groups on the silica surfaces.[59] If only the distributions of silicon functionalities need to be characterized, 1D spectra may be sufficient. In this context, DNP enhancement is clearly beneficial, especially for qualitative characterization.[23–25] For PUP-MSN samples, a high-quality DNP-CP-MAS spectrum (Fig. 1b) could be acquired in 22 min at 9.4 T, yielding a similar S/N ratio as a conventional $^{1}H \rightarrow {}^{29}Si$ CP-MAS spectrum (Fig. 5a) acquired at 14.1 T with a much longer acquisition time of 5.5 h. The change in line shape in the DNP spectrum can be attributed to the much shorter τ_{CP} contact.

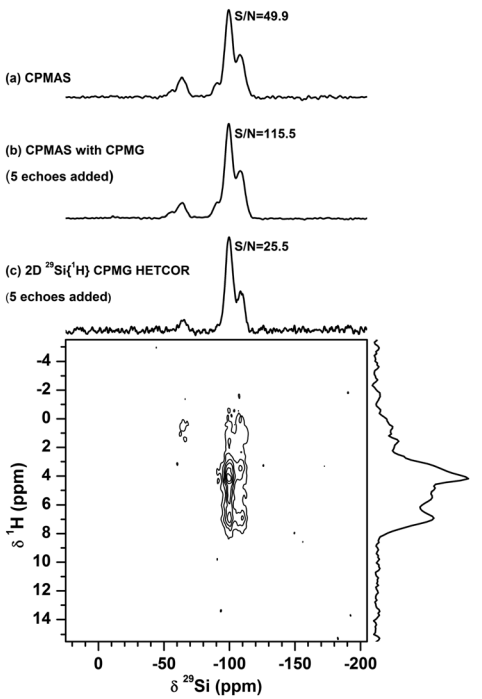

Fig. 5 The $^{1}H \rightarrow {}^{29}Si$ CP-MAS spectra for dry-RT-off obtained with (a) 1D conventional CP-MAS, (b) 1D CPMG-enhanced CP-MAS, and (c) 2D CPMG-enhanced HETCOR. The spectra were obtained at 14.1 T with ν_R = 40 kHz, τ_{CP} = 7 ms, ν_{RF}^{Si} = 100 kHz during CP and π pulses, ν_{RF}^{H} = 125 during π/2 pulse and 60 kHz during CP, τ_{CPMG} = 5 ms, and N_{CPMG} = 5. The 1D spectra were acquired in 5 h 30 min each. In the 2D experiment, the acquisition involved 64 increments, with 400 scans per increment, Δt_1 = 50 μs, requiring a total acquisition time = 17 h 45 min. The ^{1}H and ^{29}Si projections are shown in the skyline mode (see caption to Fig. 4).

5. Conclusions

We assessed various contributions to the signal enhancement obtained in DNP-CP-MAS studies of functionalized mesoporous silica nanoparticles (PUP-MSNs) and compared the results with conventional room-temperature CP-MAS measurements on the same systems. When comparing 1D CP-MAS experiments performed at low temperature (around 100 K), the sensitivity enhancement factors attributable to microwave irradiation $\varepsilon_{on/off}^{time}(^{13}C) = \varepsilon_{on/off}^{time}(^{29}Si)$ = 23 (see Table 3) exceeded the real DNP sensitivity enhancement factors corrected for quenching and changes in relaxation ($\varepsilon_{DNP}^{time}(^{13}C)$ = 5.5 and $\varepsilon_{DNP}^{time}(^{29}Si)$ = 8.3). However, the global sensitivity enhancements, adjusted for comparison with conventional 1D CP-MAS at room temperature, were even higher ($\varepsilon_{global}^{time}(^{13}C)$ = 23 and $\varepsilon_{global}^{time}(^{29}Si)$ = 45). These results confirm that DNP is useful to probe small surface areas and surface species with low concentrations. The imminent development of high-field DNP and improvements of polarizing agents will likely afford higher sensitivity gains and enable novel applications. Solvent-free approaches to DNP should eliminate perturbations due to frozen water which can affect the structure, reactivity, intermolecular interactions and dynamics on silica surfaces. Two-dimensional correlation studies of such materials, combined with indirect detection and CPMG acquisition, which recently became feasible (albeit time consuming) at room temperature should become possible at low temperatures. These techniques will necessitate faster spinning at low temperatures, and thus better control of frictional heating.[39] Possible adverse consequences of fast spinning may include quenching of spin diffusion and losses of DNP efficiency due to modulations of ESR frequencies and the resulting crossings of energy levels.[45,46]

Appendix

A.1. Enhancement factor ε^{scan} in the case of partial saturation

For $\tau_{RD} < 5T_1$, the experimentally determined value $S(\tau_{RD})$ should be corrected to account for partial saturation. Since the recycle delay τ_{RD} is much longer that the contact time and the duration of signal acquisition, the duration of each scan is roughly equal to τ_{RD} and

$$S(\tau_{RD}) = S(\infty)\{1\text{-}\exp[-\tau_{RD}/T_1]\}. \quad (A.1)$$

Thus, the general expression for the enhancement per scan is given by

$$\varepsilon^{\text{scan}}(\text{A; B}) = \frac{S_{\text{A}}(\tau_{\text{RD}}(\text{A}))}{S_{\text{B}}(\tau_{\text{RD}}(\text{B}))} \frac{\{1-\exp[-\tau_{\text{RD}}(\text{B})/T_1(\text{B})]\}}{\{1-\exp[-\tau_{\text{RD}}(\text{A})/T_1(\text{A})]\}} \frac{N_{\text{B}}}{N_{\text{A}}}. \quad \text{(A.2)}$$

A.2. Proof of eqn (2)

The enhancement factor, $\varepsilon^{\text{scan}}$(A; B), defined by eqn (1), can be written as

$$\varepsilon^{\text{scan}}(\text{A; B}) = \varepsilon^{\text{intensity}}(\text{A; B})\ \varepsilon^{\text{noise}}(\text{A; B}), \quad \text{(A.3)}$$

where the enhancement factor for signal intensity is

$$\varepsilon^{\text{intensity}}(\text{A; B}) = \frac{S_{\text{A}}(\infty)}{S_{\text{B}}(\infty)} \quad \text{(A.4)}$$

and, correspondingly,

$$\varepsilon^{\text{noise}}(\text{A; B}) = \frac{N_{\text{B}}}{N_{\text{A}}}. \quad \text{(A.5)}$$

In the presence of line broadening, one should consider the enhancement of the integrated intensities (II)

$$\varepsilon^{\text{integral}}(\text{A; B}) = \frac{\text{II}_{\text{A}}(\infty)}{\text{II}_{\text{B}}(\infty)}. \quad \text{(A.6)}$$

For a Gaussian or Lorentzian lineshape, the integrated intensity II is proportional to the product of the intensity S and the full-width at half maximum (FWHM)

$$\text{II} = \alpha \times S \times \text{FWHM}, \quad \text{(A.7)}$$

where $\alpha = 0.5\sqrt{\pi/\ln 2}$ for a Gaussian lineshape and $\pi/2$ for a Lorentzian lineshape. Therefore, in order to emphasize the contributions of the line broadening to $\varepsilon^{\text{scan}}$(A; B), eqn (A.3) can be recast as eqn (2) with

$$\varepsilon^{\text{LW}}(\text{A; B}) = \frac{\text{FWHM}_{\text{B}}(\infty)}{\text{FWHM}_{\text{A}}(\infty)}. \quad \text{(A.8)}$$

For a Lorentzian lineshape, $\text{FWHM} = \left(\pi T_2^*\right)^{-1}$ and ε^{LW}(A; B) is equal to the ratio of T_2^*'s.

A.3. Proof of eqn (3)

The sensitivity, $(\text{S/N})^{\text{time}}$, (*i.e.* the signal-to-noise per unit of time) is given by

$$(\text{S/N})^{\text{time}} = \frac{S(\tau_{\text{RD}})}{N}\sqrt{\frac{1}{\tau_{\text{RD}}}} = \frac{S(\infty)}{N}[1-\exp(-\tau_{\text{RD}}/T_1)]\sqrt{\frac{1}{\tau_{\text{RD}}}}. \quad \text{(A.9)}$$

Since the maximum $(\text{S/N})^{\text{time}}$ is achieved for $\tau_{\text{RD}} \sim 1.3T_1$ if one uses a simple 90° excitation pulse,[60] or alternatively for CP with $\tau_{\text{RD}} \sim 1.3T_1(^1\text{H})$, we can define the optimal sensitivity as

$$(\text{S/N})^{\text{time}}_{\text{opt}} = \frac{S(\infty)}{N}\frac{[1-\exp(-1.3)]}{\sqrt{1.3}}\sqrt{\frac{1}{T_1}}. \quad \text{(A.10)}$$

The sensitivity enhancement factor is defined as

$$\varepsilon^{\text{time}}(\text{A; B}) = \frac{(S_{\text{A}}/N_{\text{A}})^{\text{time}}_{\text{opt}}}{(S_{\text{B}}/N_{\text{B}})^{\text{time}}_{\text{opt}}}. \quad \text{(A.11)}$$

Substituting eqn (A.10) into eqn (A.11) leads to eqn (3).

Acknowledgements

This research was supported at the Ames Laboratory by the U.S. Department of Energy, Office of Basic Energy Sciences. Ames Laboratory is operated for the U.S. Department of Energy by Iowa State University under Contract No. DE-AC02-07CH11358. In Lille, this research was supported by the Region Nord/Pas de Calais, Europe (FEDER), the CNRS, the French Ministry of Science, FR-3050, USTL, ENSCL, Bruker BioSpin, MPNS COST Action EUROHyperPOL TD1103, and the ANR under contract 2010-JCJC-0811-01. In Lausanne, this work was supported by the Commission for Technology and Innovation (CTI), the Swiss National Science Foundation (SNSF) and the EPFL.

Notes and references

1 A. Abragam, *Principles of Nuclear Magnetism*, Oxford, NY, 1961.
2 A. W. Overhauser, *Phys. Rev.*, 1953, **92**, 411–415.
3 T. R. Carver and C. P. Slichter, *Phys. Rev.*, 1953, **92**, 212–213.
4 H. Lock, G. E. Maciel and C. E. Johnson, *J. Mater. Res.*, 1992, **7**, 2791–2797.
5 R. A. Wind, in *Encyclopedia of NMR*, ed. D. M. Grant and R. K. Harris, John Wiley, Chichester, 1996, pp. 1798–1807.
6 S. Sabchevski, T. Idehara, S. Mitsudo and T. Fujiwara, *Int. J. Infrared Millimeter Waves*, 2005, **26**, 1241–1264.
7 C. D. Joye, R. G. Griffin, M. K. Hornstein, K. N. Hu, K. E. Kreischer, M. Rosay, M. A. Shapiro, J. R. Sirigiri, R. J. Temkin and P. P. Woskov, *IEEE Trans. Plasma Sci.*, 2006, **34**, 518–523.
8 M. Rosay, J. C. Lansing, K. C. Haddad, W. W. Bachovchin, J. Herzfeld, R. J. Temkin and R. G. Griffin, *J. Am. Chem. Soc.*, 2003, **125**, 13626–13627.
9 K. N. Hu, H. H. Yu, T. M. Swager and R. G. Griffin, *J. Am. Chem. Soc.*, 2004, **126**, 10844–10845.
10 C. Song, K.-N. Hu, C.-G. Joo, T. M. Swager and R. G. Griffin, *J. Am. Chem. Soc.*, 2006, **128**, 11385–11390.
11 A. B. Barnes, M. L. Mak-Jurkauskas, Y. Matsuki, V. S. Bajaj, P. C. A. van der Wel, R. DeRocher, J. Bryant, J. R. Sirigiri, R. J. Temkin, J. Lugtenburg, J. Herzfeld and R. G. Griffin, *J. Magn. Reson.*, 2009, **198**, 261–270.
12 K.-N. Hu, C. Song, H.-H. Yu, T. M. Swager and R. G. Griffin, *J. Chem. Phys.*, 2008, **128**, 052302.
13 C. F. Hwang and D. A. Hill, *Phys. Rev. Lett.*, 1967, **19**, 1011–1014.
14 T. Maly, G. T. Debelouchina, V. S. Bajaj, K.-N. Hu, C.-G. Joo, M. L. Mak-Jurkauskas, J. R. Sirigiri, P. C. A. van der Wel, J. Herzfeld, R. J. Temkin and R. G. Griffin, *J. Chem. Phys.*, 2008, **128**, 052211.
15 P. C. A. van der Wel, K.-N. Hu, J. Lewandowski and R. G. Griffin, *J. Am. Chem. Soc.*, 2006, **128**, 10840–10846.

16 M. L. Mak-Jurkauskas, V. S. Bajaj, M. K. Hornstein, M. Belenky, R. G. Griffin and J. Herzfeld, *Proc. Natl. Acad. Sci. U. S. A.*, 2008, **105**, 883–888.
17 V. S. Bajaj, M. L. Mak-Jurkauskas, M. Belenky, J. Herzfeld and R. G. Griffin, *Proc. Natl. Acad. Sci. U. S. A.*, 2009, **106**, 9244–9249.
18 A. H. Linden, S. Lange, W. T. Franks, U. Akbey, E. Specker, B.-J. van Rossum and H. Oschkinat, *J. Am. Chem. Soc.*, 2011, **133**, 19266–19269.
19 T. Jacso, W. T. Franks, H. Rose, U. Fink, J. Broecker, S. Keller, H. Oschkinat and B. Reif, *Angew. Chem., Int. Ed.*, 2012, **51**, 432–435.
20 M. Renault, S. Pawsey, M. P. Bos, E. J. Koers, D. Nand, R. Tommassen-van Boxtel, M. Rosay, J. Tommassen, W. E. Maas and M. Baldus, *Angew. Chem., Int. Ed.*, 2012, **51**, 2998–3001.
21 H. Takahashi, D. Lee, L. Dubois, M. Bardet, S. Hediger and G. De Paepe, *Angew. Chem., Int. Ed.*, 2012, **51**, 11766–11769.
22 A. J. Rossini, A. Zagdoun, F. Hegner, M. Schwarzwalder, D. Gajan, C. Coperet, A. Lesage and L. Emsley, *J. Am. Chem. Soc.*, 2012, **134**, 16899–16908.
23 A. Lesage, M. Lelli, D. Gajan, M. A. Caporini, V. Vitzthum, P. Mieville, J. Alauzun, A. Roussey, C. Thieuleux, A. Mehdi, G. Bodenhausen, C. Coperet and L. Emsley, *J. Am. Chem. Soc.*, 2010, **132**, 15459–15461.
24 M. Lelli, D. Gajan, A. Lesage, M. A. Caporini, V. Vitzthum, P. Mieville, F. Heroguel, F. Rascon, A. Roussey, C. Thieuleux, M. Boualleg, L. Veyre, G. Bodenhausen, C. Coperet and L. Emsley, *J. Am. Chem. Soc.*, 2011, **133**, 2104–2107.
25 O. Lafon, M. Rosay, F. Aussenac, X. Lu, J. Trebosc, O. Cristini, C. Kinowski, N. Touati, H. Vezin and J.-P. Amoureux, *Angew. Chem., Int. Ed.*, 2011, **50**, 8367–8370.
26 A. J. Rossini, A. Zagdoun, M. Lelli, J. Canivet, S. Aguado, O. Ouari, P. Tordo, M. Rosay, W. E. Maas, C. Coperet, D. Farrusseng, L. Emsley and A. Lesage, *Angew. Chem., Int. Ed.*, 2012, **51**, 123–127.
27 K. R. Thurber, W.-M. Yau and R. Tycko, *J. Magn. Reson.*, 2010, **204**, 303–313.
28 V. Vitzthum, F. Borcard, S. Jannin, M. Morin, P. Mieville, M. A. Caporini, A. Sienkiewicz, S. Gerber-Lemaire and G. Bodenhausen, *ChemPhysChem*, 2011, **12**, 2929–2932.
29 A. J. Rossini, A. Zagdoun, M. Lelli, D. Gajan, F. Rascon, M. Rosay, W. E. Maas, C. Coperet, A. Lesage and L. Emsley, *Chem. Sci.*, 2012, **3**, 108–115.
30 S. Lange, A. H. Linden, U. Akbey, W. T. Franks, N. M. Loening, B.-J. van Rossum and H. Oschkinat, *J. Magn. Reson.*, 2012, **216**, 209–212.
31 Y. Ishii and R. Tycko, *J. Magn. Reson.*, 2000, **142**, 199–204.
32 J. W. Wiench, C. E. Bronnimann, V. S. Y. Lin and M. Pruski, *J. Am. Chem. Soc.*, 2007, **129**, 12076–12077.
33 J. Trebosc, J. W. Wiench, S. Huh, V. S. Y. Lin and M. Pruski, *J. Am. Chem. Soc.*, 2005, **127**, 7587–7593.
34 J. W. Wiench, V. S. Y. Lin and M. Pruski, *J. Magn. Reson.*, 2008, **193**, 233–242.
35 S. Huh, J. W. Wiench, J. C. Yoo, M. Pruski and V. S. Y. Lin, *Chem. Mater.*, 2003, **15**, 4247–4256.
36 I. I. Slowing, B. G. Trewyn and V. S. Y. Lin, *J. Am. Chem. Soc.*, 2007, **129**, 8845–8849.
37 S. Stoll and A. Schweiger, *J. Magn. Reson.*, 2006, **178**, 42–55.
38 A. B. Barnes, G. De Paepe, P. C. A. van der Wel, K. N. Hu, C. G. Joo, V. S. Bajaj, M. L. Mak-Jurkauskas, J. R. Sirigiri, J. Herzfeld, R. J. Temkin and R. G. Griffin, *Appl. Magn. Reson.*, 2008, **34**, 237–263.
39 M. Rosay, L. Tometich, S. Pawsey, R. Bader, R. Schauwecker, M. Blank, P. M. Borchard, S. R. Cauffman, K. L. Felch, R. T. Weber, R. J. Temkin, R. G. Griffin and W. E. Maas, *Phys. Chem. Chem. Phys.*, 2010, **12**, 5850–5860.
40 P. P. Woskov, V. S. Bajaj, M. K. Hornstein, R. J. Temkin and R. G. Griffin, *IEEE Trans. Microwave Theory Tech.*, 2005, **53**, 1863–1869.
41 K. R. Thurber and R. Tycko, *J. Magn. Reson.*, 2009, **196**, 84–87.
42 O. Lafon, A. S. L. Thankamony, T. Kobayashi, V. V. Carnevale, I. I. Slowing, K. Kandel, H. Vezin, J.-P. Amoureux, G. Bodenhausen and M. Pruski, *J. Phys. Chem. C*, 2013, **117**, 1375–1382.
43 K.-N. Hu, G. T. Debelouchina, A. A. Smith and R. G. Griffin, *J. Chem. Phys.*, 2011, **134**, 125105.
44 E. A. Nanni, A. B. Barnes, Y. Matsuki, P. P. Woskov, B. Corzilius, R. G. Griffin and R. J. Temkin, *J. Magn. Reson.*, 2011, **210**, 16–23.
45 K. R. Thurber and R. Tycko, *J. Chem. Phys.*, 2012, **137**, 084508.
46 F. Mentink-Vigier, U. Akbey, Y. Hovav, S. Vega, H. Oschkinat and A. Feintuch, *J. Magn. Reson.*, 2012, **224**, 13–21.
47 B. M. Fung, A. K. Khitrin and K. Ermolaev, *J. Magn. Reson.*, 2000, **142**, 97–101.
48 S. Balayssac, I. Bertini, A. Bhaumik, M. Lelli and C. Luchinat, *Proc. Natl. Acad. Sci. U. S. A.*, 2008, **105**, 17284–17289.
49 V. Vitzthum, M. A. Caporini and G. Bodenhausen, *J. Magn. Reson.*, 2010, **205**, 177–179.
50 G. R. Khutsishvili, *Sov. Phys. Usp.*, 1969, **11**, 802–815.
51 A. A. Smith, B. Corzilius, A. B. Barnes, T. Maly and R. G. Griffin, *J. Chem. Phys.*, 2012, **136**, 15101.
52 D. S. Wollan, *Phys. Rev. B: Condens. Matter Mater. Phys.*, 1976, **13**, 3671–3685.
53 D. Shimon, Y. Hovav, A. Feintuch, D. Goldfarb and S. Vega, *Phys. Chem. Chem. Phys.*, 2012, **14**, 5729–5743.
54 T. A. Siaw, S. A. Walker, B. D. Armstrong and S.-I. Han, *J. Magn. Reson.*, 2012, **221**, 5–10.
55 V. S. Bajaj, P. C. A. van der Wel and R. G. Griffin, *J. Am. Chem. Soc.*, 2009, **131**, 118–128.
56 C. A. Fyfe and D. H. Brouwer, *J. Am. Chem. Soc.*, 2004, **126**, 1306–1307.
57 A. S. Lilly Thankamony, O. Lafon, X. Lu, F. Aussenac, M. Rosay, J. Trebosc, H. vezin and J.-P. Amoureux, *Appl. Magn. Reson.*, 2012, **43**, 237–250.
58 J. W. Wiench, Y. S. Avadhut, N. Maity, S. Bhaduri, G. K. Lahiri, M. Pruski and S. Ganapathy, *J. Phys. Chem. B*, 2007, **111**, 3877–3885.
59 K. Mao, T. Kobayashi, J. W. Wiench, H.-T. Chen, C.-H. Tsai, V. S. Y. Lin and M. Pruski, *J. Am. Chem. Soc.*, 2010, **132**, 12452–12457.
60 M. Pons, M. Feliz and E. Giralt, *J. Magn. Reson.*, 1988, **78**, 314–320.

